Optical properties and dynamic process in metal ions doped on CdSe quantum dots sensitized solar cells

Ha Thanh Tung[1] and Dang Huu Phuc[2,3,*]

[1]*Institute of Research and Development, Duy Tan University, Da Nang, Vietnam*
[2]*Theoretical Physics Research Group, Advanced Institute of Materials Science, Ton Duc Thang University, Ho Chi Minh City, Vietnam*
[3]*Faculty of Applied Sciences, Ton Duc Thang University, Ho Chi Minh City, Vietnam*
**Corresponding author: danghuuphuc@tdt.edu.vn*

Received March 14, 2018; accepted May 8, 2018; posted online July 2, 2018

In recent years, the nanostructure for solar cells have attracted considerable attention from scientists as a result of a promising candidate for low cost devices. In this work, quantum dots sensitized solar cells with effective performance based on a co-sensitized CdS/CdSe:Mn^{2+} (or Cu^{2+}) nanocrystal, which was made by successive ionic layer absorption and reaction, are discussed. The optical, physical, chemical, and photovoltaic properties of quantum dots sensitized solar cells were sensitized to Mn^{2+} and Cu^{2+} dopants. Therefore, the short current (J_{SC}) of the quantum dot sensitized solar cells is boosted dramatically from 12.351 mA/cm^2 for pure CdSe nanoparticles to 18.990 mA/cm^2 for Mn^{2+} ions and 19.915 mA/cm^2 for Cu^{2+} ions. Actually, metal dopant extended the band gap of pure CdSe nanoparticles, reduced recombination, enhanced the efficiency of devices, and improved the charge transfer and collection. In addition, Mn^{2+} and Cu^{2+} dopants rose to the level of the conduction band of pure CdSe nanoparticles, which leads to the reduction of the charge recombination, enhances the light-harvesting efficiency, and improves the charge diffusion and collection. The results also were confirmed by the obtained experimental data of photoluminescence decay and electrochemical impedance spectroscopy.

OCIS codes: 250.4745, 260.2160.
doi: 10.3788/COL201816.072501.

For decades, quantum dot sensitized solar cells (QDSSCs) based on quantum dots (QDs) have been of considerable interest as promising candidates to replace the dye sensitized solar cells (DSSCs) because QDs have potential functions, such as a high extinction coefficient, tunable bandgaps, a large intrinsic dipole moment, generation of multiple excitons[1], and low processing cost compared to organic dyes[2,3]. The QDs were used in QDSSCs as sensitizers that include PbS[4,5], PbSeS[6], CdS[7], CdSe[8], CdTe[9], and ZnS[10]. The highest efficiency, which was achieved by Jara *et al.*, was approximately 2.51% for $CuInS_2$[11], because the electrons in the conduction band (CB) of the QDs move to the electrolyte and recombine or get blocked. Moverover, tandem multilayers can increase the power conversion efficiency in the QDSSCs. For instance, Jung *et al.* studied the QDSSCs based on the TiO_2/CdS/$CuInS_2$ tandem multilayers, and the power conversion efficiency was about 1.47%[12,13]. This photovoltaic performance was higher than those of the lonely CdS and $CuInS_2$ QDs. However, the efficiency was still minor because of the increased combination processes at the QDs/TiO_2 surface and plenty of electrons moving to the electrolyte.

In order to boost the conversion efficiency of photovoltaics, TiO_2/CdS/CdSe/ZnS multiplayers have been studied to improve the short current (J_{SC}) density of solar cells[14,15]. As a result, photoanodes can absorb a large amount of photons from the UV to the visible region. Furthermore, the ZnS coating forms a potential barrier between the QDs and the electrolyte, blocking the electrons in the CB transfer from the QDs to the electrolyte and reducing the defect states in the QDs[16]. In recent years, researchers reported the result of metals doped on nanoparticles, such as Hg^{2+} on PbS[17] and Mn^{2+} on CdS[18]. As a result, it could boost the J_{SC} density and efficiency of solar cells as compared with pure CdS and PbS QDs and CdSe QDs due to enhancing the light harvesting, generation, collection, and injection of the excited electrons between nanoparticles and TiO_2 film[19,20]. The performance of CdSe QDSSCs is much higher than that of the sulfide QDSSCs[21–25]. Therefore, metal ions doped on pure CdSe QDs can be a useful way for high efficiency QDSSCs[26,27].

As mentioned above, QDSSCs based on metal ions doped on CdSe nanoparticles with the different compositions of the Mn^{2+} and the Cu^{2+} are achieved by successive ionic layer adsorption and reation (SILAR). Moreover, the significant effects of the X dopant on optical, physical, chemical, and photovoltaic properties of films can be studied by the UV-visible (UV-Vis) spectra and Tauc plots to determine the band gap, CB, and valence band (VB) positions of metal ions. In the same way, the dynamic processes of QDSSCs are also studied through photoluminescence (PL) decay and electrochemical impedance spectra (EIS).

In this experiment, a fluorine-doped tin oxide (FTO) glass substrate with sheet resistance 7 $\Omega \cdot \mathrm{sq}^{-2}$ was used for the photoanode and the counter electrode. First, the FTO substrate was cleaned in ethanol for 30 min by

ultrasonics, followed by deionized (DI) water for 15 min. The nanoporous TiO_2 film was made on the well-cleaned substrate by the print method followed by sintering at 500°C for 30 min. **TiO_2/CdS film**: TiO_2 film was dipped into a $Cd(CH_3COO)_2 \cdot 2H_2O$ ethanol solution (0.1 M, 1 M = 1 mol/L) for 5 min, rinsed with ethanol, and dried, then successively dipped into a $Na_2S \cdot 9H_2O$ methanol solution (0.1 M) for another 5 min, rinsed with methanol, and dried. The two-step dipping procedure was termed as one SILAR cycle. The process was repeated for three times, and the obtained TiO_2 film decorated with CdS QDs was named as the TiO_2/CdS film[28–31]. **TiO_2/CdS/CdSe:Mn^{2+} film**: TiO_2/CdS film was dipped into a mixed $Cd(CH_3COO)_2 \cdot 2H_2O$ and $Mn(CH_3COO)_2 \cdot 2H_2O$ ethanol solution for 5 min, rinsed with ethanol, and dried, then successively dipped into a Se source methanol solution for 5 min, rinsed with methanol, and dried. The two-step dipping procedure was termed as one SILAR cycle. The process was repeated for three times as CdSe:$Mn^{2+}(x)$ with x representing the Mn^{2+}-doped molar concentration at 5%, 10%, 20%, 30%, and 40%. **TiO_2/CdS/CdSe:Cu^{2+} film**: Sodium selenosulphate (Na_2SeSO_3) 0.3 M was used as the Se source for SILAR. The Na_2SeSO_3 aqueous solution was prepared by refluxing Se (0.3 M) in an aqueous solution of Na_2SO_3 (0.6 M) and NaOH (1M) at 70°C for about 7 h. To accommodate the doping of the Cu^{2+} ion, relevant molar concentrations of 0.1 mM, 0.2 mM, 0.3 mM, 0.4 mM, and 0.5 mM of $Cu(NO_3)_2 \cdot 3H_2O$ were mixed with a $Cd(CH_3COO)_2 \cdot 2H_2O$ anion source. The SILAR process of CdSe and Cu^{2+}-doped CdSe QDs was similar to that of CdS, except that 15 min and 50°C were required for dipping the TiO_2/CdS film in the Na_2SeSO_3 aqueous solution. Different electrodes were named as CdSeCu$^{2+}(y)$ with y representing the Cu^{2+}-doped molar concentration and number of the SILAR cycle, respectively. Finally, the electrode was coated with a ZnS passivation layer by dipping alternately into 0.1 M $Zn(NO_3)_2 \cdot 6H_2O$ and 0.1 M $Na_2S \cdot 9H_2O$ DI water solution for 5 min each. This process was repeated twice to get the optimal thickness[28–31].

A polysulfide solution was made by dissolving 0.5 M $Na_2S \cdot 9H_2O$, 0.2 M S, and 0.2 M KCl in DI water/methanol (7:3 by volume). The Cu_2S counter electrode was synthesized through chemical bath deposition according to Ref. [32]. Briefly, 0.24 g $CuSO_4$ was dissolved in 60 mL DI in a glass bottle. N_2 was bubbled through the water for 10 min to remove the dissolved oxygen from the system. Then, 0.37 g $Na_2S_2O_3 \cdot 5H_2O$ was mixed in the solution, and the color turned to light green. Afterwards, a clean FTO glass was immersed in the solution with its conductive surface facing down and had an angle against the wall. The system was then settled in the water bath of 90°C and kept for 1 h. The Cu_2S crystal would directly grow onto the conductive surface of the FTO glass. Finally, the as-prepared Cu_2S-coated FTO glass sample was rinsed with DI water and dried in air. The post-heating treatment was carried out in an N_2 atmosphere at 200°C for 30 min.

The morphologies of the samples were investigated using scanning electron microscopy (SEM). The crystal structure was analyzed using an X-ray diffractometer (Philips, PANalytical X'Pert, CuKα radiation). The absorption properties of the samples were investigated using a diffuse reflectance UV–Vis spectrometer (JASCO V-670). Photocurrent–voltage measurements were performed on a Keithley 2400 source meter using simulated air mass (AM) 1.5 sunlight with an output power of 100 mW · cm^{-2} produced by a solar simulator (Solarena, Sweden). The EIS was carried out with the use of an impedance analyzer (ZAHNER CIMPS). The PL spectra were measured by an excitation wavelength of 430 nm at room temperature using a Shimadzu luminescence spectrometer RF-5301PC.

As far as previous work is concerned, the TiO_2 nanoparticles were deposited on the FTO substrate[33]. Therefore, we only discussed the details based on the deposition of CdS, CdSe:X nanoparticles on the FTO/TiO_2. The typical field emission SEM (FE-SEM) images of co-sensitized CdS/CdSe:Mn^{2+} (or Cu^{2+}) show that the mood surface morphology [Figs. 1(a) and 1(d), respectively] and nanoparticles are nearly spherical with an average cluster size of over 70 nm, which agrees well with the X-ray diffraction (XRD) analysis. Besides, the thicknesses of photoanode films are determined as approximately 12.056 μm (FTO: 0.563 μm, TiO_2: 10.653 μm, CdS/CdSe:Mn^{2+}: 720 nm, and ZnS: 120 nm) for CdSe:Mn^{2+} and 12.675 μm (FTO: 0.563 μm, TiO_2: 11.377 μm, CdS/CdSe:Mn^{2+}: 615 nm, and ZnS: 120 nm) for CdSe:Cu^{2+} by cross-sections [Figs. 1(b) and 1(e), respectively]. The compositional energy dispersive X-ray (EDX) analysis of the CdSe:X was shown in Figs. 1(c) and 1(f), and the experimental data was recorded in Tables 1 and 2, which proves the presence of Mn^{2+} and Cu^{2+} dopants in photoanodes. As can be seen from Figs. 1(g) and 1(h), they are the same structures of TiO_2, CdS, and CdSe:Mn^{2+} (Cu^{2+}). It is immediately obvious that the XRD patterns of TiO_2/CdS/CdSe:Mn^{2+}/ZnS and TiO_2/CdS/CdSe:Cu^{2+}/ZnS appear at the peaks at the 47.4° and 55.7° positions, corresponding to the (200) and (111) planes, which indicates an upstanding ZnS blend. It is completely suitable with the Joint Committee on Powder Diffraction Standards (JCPDS) No. 05-5666. It also shows that the peaks at the 43.3° and 50.0° positions correspond to the (220) and (311) planes of the CdSe zinc blend (JCPDS No. 88-2346), and the peaks at 30.7°, 50.6°, and 67.2° correspond to the (101), (112), and (203) planes of the CdS zinc blend (JCPDS No. 41-1019), respectively. Finally, the left peaks of XRD characterize the TiO_2 anatase (JCPDS No. 21-1272). This implies that CdS, CdSe:Cu^{2+}(Mn^{2+}), and ZnS nanoparticles have been absorbed on TiO_2 films.

In QDSSCs, a band alignment of nanoparticles in an anode is quite necessary for us to explain the diffraction and movement of excited electrons in CB levels of a semiconductor. The band gap of CdSe bulk, which can be absorbed in the visible region, is approximately 1.76 eV[33],

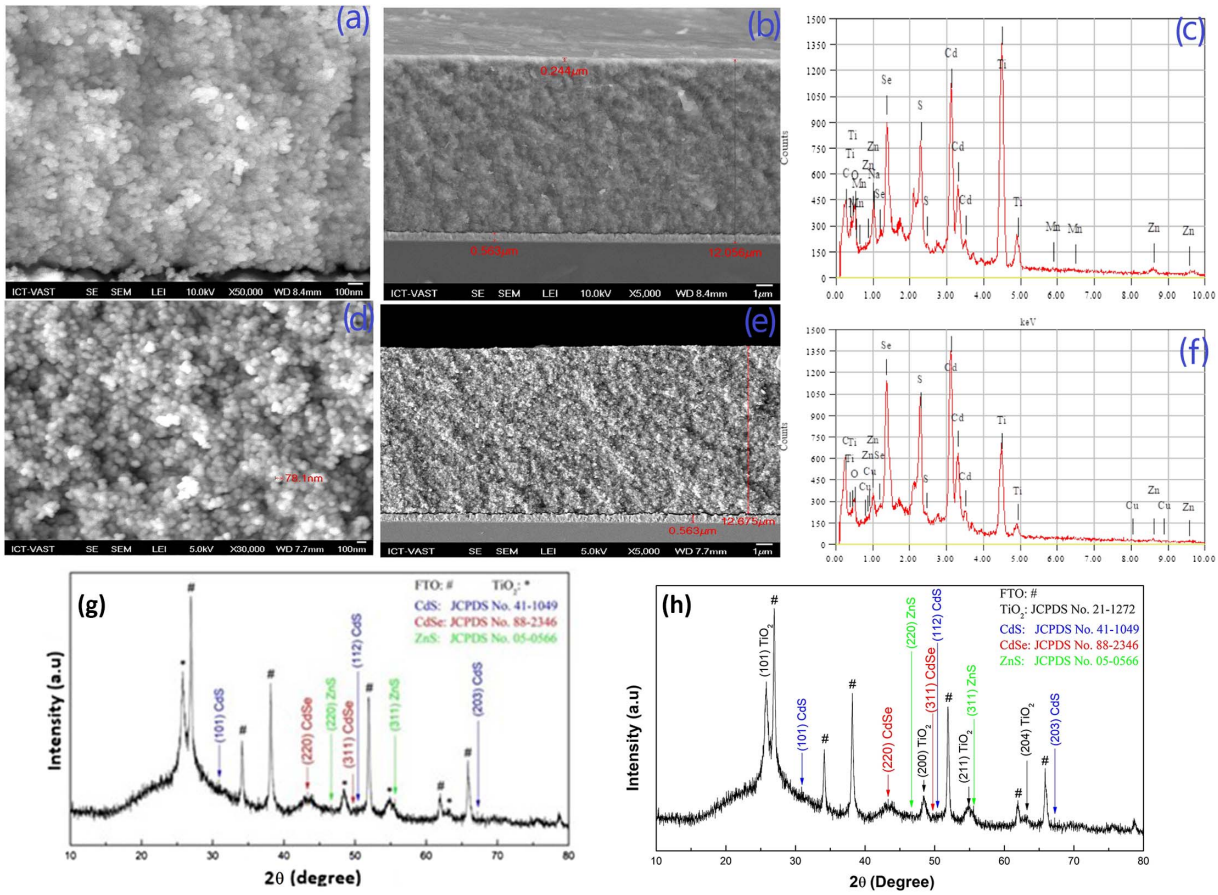

Fig. 1. (a), (d) FE-SEM image at 100 nm, (b), (e) cross-section at 1 μm, and (c), (f) EDX pattern of co-sensitized CdS/CdSe:Mn^{2+} (or Cu^{2+}). (g), (h) XRD patterns of co-sensitized CdS/CdSe:Mn^{2+} (or Cu^{2+}) QDSSCs.

Table 1. Composition of TiO_2/CdS/CdSe:Cu^{2+}/ZnS

Elements		Energy (keV)	Mass fraction (%)	Atom fraction (%)
C	K	0.277	5.09	24.37
O	K	0.525	0.77	2.78
S	K	2.307	8.25	14.78
Ti	K	4.508	13.85	16.62
Cu	K	8.040	0.45	0.41
Zn	K	8.630	0.66	0.58
Se	L	1.379	19.39	14.11
Cd	L	3.133	51.53	26.35

Table 2. Composition of TiO_2/CdS/CdSe:Mn^{2+}/ZnS

Elements		Energy (keV)	Mass fraction (%)	Atom fraction (%)
C	K	0.277	1.00	4.31
O	K	0.525	1.82	5.91
Na	K	1.041	1.07	2.42
Al	K	1.486	1.10	2.13
Si	K	1.739	0.83	1.54
S	K	2.307	7.38	11.96
Ti	K	4.508	50.71	55.04
Cd	L	3.133	36.09	16.69

but the CB of CdSe becomes lower than that of TiO_2. Therefore, injection of the excited electrons into TiO_2 film becomes hard. On the other hand, the CB of CdS bulk is higher than that of TiO_2, which is the driving force, making the movement of the excited electrons to TiO_2 easier[34]. Co-sensitized CdS/CdSe can significantly improve the performance of QDSSCs[34,35]. In addition, Lee and co-workers said that the Fermi energy of CdSe nanoparticles shifted to above, while that of CdS nanoparticles shifted down, as CdS/CdSe co-sensitized to make the TiO_2 < CdS < CdSe structure[24]. Therefore, the excited electrons are able to easily transfer from CdSe, CdS nanoparticles to TiO_2.

Moreover, the CB and VB positions of CdS and CdSe nanoparticles can be determined by the Tauc equation to demonstrate the abovementioned. The CB and VB of materials can be calculated if the electron affinity energy and the ionization energy are known. Similarly, the CB, VB of

CdS and CdSe can be determined by the Tauc equation as follows[36–38]:

$$E^0_{\mathrm{CB}} = E_e - X + 0.5E_g, \tag{1}$$

where

$$X = (x^x_{\mathrm{Cd}} \times x^y_S \times x^z_{\mathrm{Se}})^{1/(x+y+z)}, \tag{2}$$

with

$$x_M = \frac{1}{2}(E^M_{\mathrm{EA}} + E^M_{\mathrm{Ion}}), \tag{3}$$

E^0_{CB} is the CB potential, E_e is a given constant equal of 4.5 eV[37–39], X is an energy parameter and depends on the elements of composition, and E_g is the band gap of materials. E_{EA} and E_{Ion} are the electron affinity energy and the ionization energy of CdS, CdSe, respectively. The values of E_{EA} and E_{Ion} for Cd, S, and Se are 0, 2.077, 2.020 eV and 8.99, 10.36, 9.75 eV, respectively. Finally, the calculated parameters are listed in Table 3.

Looking at Fig. 2(a), it is immediately obvious that the absorbances of the CdSe:Mn^{2+} and the CdSe:Cu^{2+} were not only much higher than that of the pure CdSe, but also significantly shifted towards the long wavelength region (red shift). For this reason, the increased absorbance of photoanodes can be contributed to the Mn^{2+}(Cu^{2+}) dopant in CdSe nanoparticles. Besides, this also implies that the energy level of the Mn^{2+}(Cu^{2+}) dopant is made in the band gap of the pure CdSe nanoparticles, corresponding to the d state of the Mn^{2+}(Cu^{2+}) dopant[39–41]. In brief, the presence of Mn^{2+}(Cu^{2+}) in CdSe nanoparticles is not only shifting towards the long wavelength region, but also the enhanced absorbance of films leading to the high performance QDSSCs.

Table 3. E_g, CB, and VB Positions of the Co-sensitized CdS/CdSe:Mn^{2+} (or Cu^{2+}) Calculated by the Tauc equation and UV-Vis Spectra

Materials	E_g (eV)	X (eV)	E_{CB} (eV)	E_{VB} (eV)
Pure CdSe	2.03	5.102	−4.08	−6.11
CdSe:Mn^{2+} (20%)	1.75	4.620	−3.74	−5.49
CdSe:Cu^{2+} (0.3%)	1.73	4.913	−4.05	−5.78

The E_g of CdS, CdSe:Mn^{2+} (or Cu^{2+}) obtained from UV-Vis spectra and the CB and VB positions of CdS, and CdSe:Mn^{2+} (or Cu^{2+}) can be determined by Tauc Eq. (1) [Fig. 2(b) and Table 3]. The E_g of the CdSe:Mn^{2+} and CdSe:Cu^{2+} nanocrystals are calculated with values of 1.75 and 1.73 eV, respectively, which are smaller than that (2.03 eV) of pure CdSe nanoparticles. Therefore, the presence of Mn^{2+}(Cu^{2+}) in CdSe nanoparticles could reduce E_g of pure CdSe, which enhances the efficiency of high harvesting. Conversely, the CB and VB levels of the CdSe:Mn^{2+} and CdSe:Cu^{2+} are estimated and listed in Table 3 with values of −3.74 and −4.05 eV, respectively, which are higher than both that (−4.08 eV) of pure CdSe and that (−4.10 eV) of the CdS nanocrystal. As a result, the Mn^{2+}(Cu^{2+}) dopant in CdSe nanoparticles facilitates the transfer of the electrons from CdSe, CdS nanoparticles to TiO_2.

Figure 3(a) shows the excited state electron radiative decay of TiO_2 film loaded with the CdSe:Mn^{2+}, CdSe:Cu^{2+}, and pure CdSe nanocrystals corresponding to 200, 203, and 206.5 ns, respectively. It is obvious that the emission decays of the CdSe:Mn^{2+} and CdSe:Cu^{2+} nanocrystals are longer than that of the pure CdSe, which indicates that the PL lifetime of pure CdSe nanoparticles can be slightly shortened by the Mn^{2+}(Cu^{2+}) dopant. In that case, there is a significant rise of J_{SC} density (Table 4) because of the increase of the injection kinetics of photogenerated electrons in nanoparticles. This result also shows a growth of the CB of CdSe:Mn^{2+}(Cu^{2+}), which is completely suitable with result of the UV-Vis spectra and references[42–45].

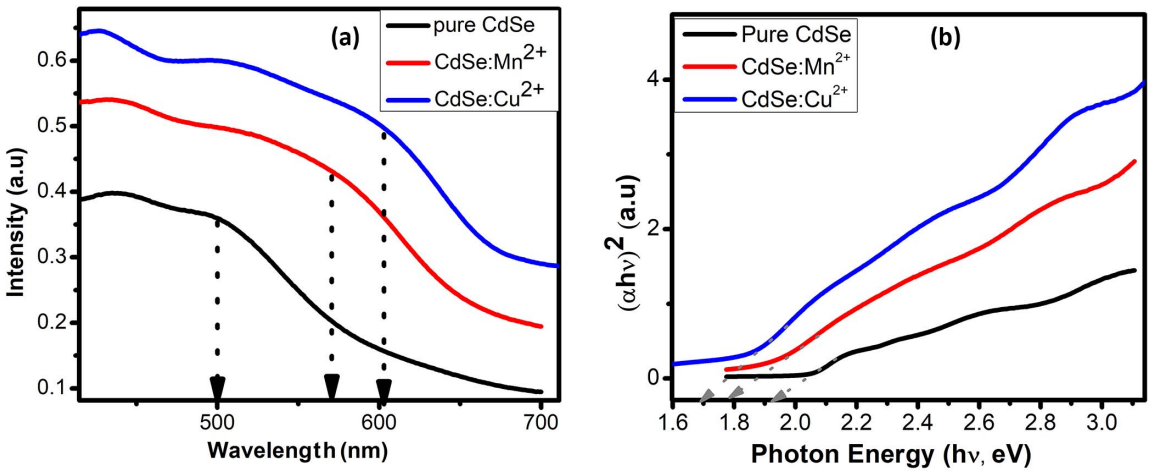

Fig. 2. (a) UV-Vis spectra and (b) $(\alpha h\nu)^2$ vs $(h\nu)$ curves of the pure CdS/CdSe and co-sensitized CdS/CdSe:Mn^{2+} (or Cu^{2+}) QDSSCs.

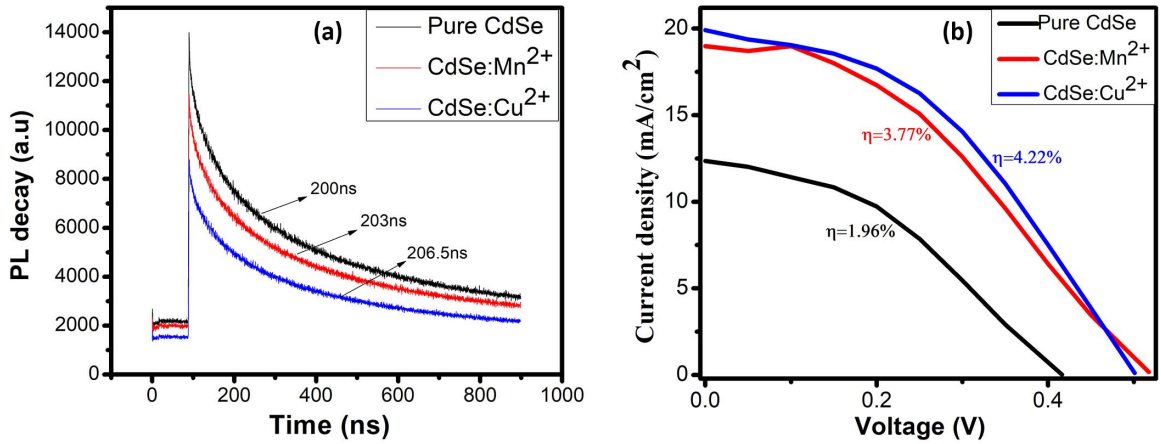

Fig. 3. (a) PL decays and (b) photocurrent density–voltage (J-V) curves of the pure CdS/CdSe and co-sensitized CdS/CdSe:Mn^{2+} (or Cu^{2+}) QDSSCs.

Table 4. Values of J-V Curves and Electrochemical Impedance Spectra of the Pure CdS/CdSe and Co-sensitized CdS/CdSe:Mn^{2+} (or Cu^{2+}) QDSSCs

Anodes	J_{SC} (mA/cm^2)	FF	V_{OC} (V)	η (%)	R_S (Ω)	R_{CE} (Ω)	R_{ct} (Ω)	C_μ (μF)
Pure CdSe	12.351	0.382	0.417	1.96	20.25	630.5	194.8	12.25
CdSe:Mn^{2+} (20%)	18.990	0.381	0.520	3.77	17.05	204.5	24.65	120.9
CdSe:Cu^{2+} (0.3%)	19.915	0.421	0.503	4.22	19.29	254.4	8.681	160.5

As far as the introduction part is concerned, QDSSCs based on co-sensitized CdS/CdSe:Mn^{2+} (or Cu^{2+}) with a concentration of Mn^{2+} at 20% and Cu^{2+} at 0.2% obtained the best optical properties. Therefore, QDSSCs were prepared and compared as concentrations of Mn^{2+} at 30% and Cu^{2+} at 0.3%. Figure 3(b) illustrates the J-V characteristics for the QDSSCs based on the different photoanodes under illumination of one sun (AM 1.5, 100 mW/cm^2), and the parameters are listed in Table 4. It is clear that the QDSSCs based on TiO_2/CdS/CdSe:Mn^{2+} (20%) and TiO_2/CdS/CdSe:Cu^{2+} (0.3%) exhibit higher performance: $J_{SC} = 18.99$ mA/cm^2, $V_{OC} = 0.381$ V, FF $= 0.52$, and $\eta = 3.77\%$, and $J_{SC} = 19.915$ mA/cm^2, $V_{OC} = 0.421$ V, FF $= 0.503$, and $\eta = 4.22\%$, respectively. As can be expected, there was a sharp increase of the current density from 12.351 to 18.99 and 19.915 mA/cm^2 after Mn^{2+}(Cu^{2+}) ions were doped on the CdSe nanoparticles, which is a main cause of the enhanced performance in the QDSSCs. The efficiency of the QDSSCs is improved as Mn^{2+}(Cu^{2+}) is doped on CdSe nanoparticles by the following reasons: firstly, an increase of light harvesting, charge transfer, and charge collection; secondly, the lifetime of co-sensitized CdS/CdSe:Mn^{2+} (or Cu^{2+}) is longer than that of pure CdS/CdSe nanoparticles. In addition, there was a rapid growth of efficiency from 1.96% to 3.77% and 4.22%.

The band alignments of TiO_2/CdS/CdSe:Mn^{2+} (or Cu^{2+}) and TiO_2/CdS/CdSe are illustrated in Fig. 4(a), and the value parameters are calculated in Table 3. It is obvious that both the CB and VB positions of CdSe:Mn^{2+} and CdSe:Cu^{2+} are higher than those of both pure CdSe and CdS nanoparticles. Therefore, the TiO_2 < CdS < CdSe:Mn^{2+} (Cu^{2+}) tandem structure is made by Mn^{2+}(Cu^{2+}) doped on pure CdSe nanoparticles. This implies that it facilitates the transfer of the electrons from CdSe nanoparticles to CdS and TiO_2, making it easier to improve the performance of the QDSSCs. Moreover, the energy levels of dopants appear in the band gap and the VB of nearly pure CdSe nanoparticles for Cu^{2+} at about 0.31 and 1.73 eV, and the VB of nearly pure CdSe nanoparticles for Mn^{2+} at approximately 0.38 and 1.8 eV, respectively. These results are definitely suitable for Refs. [46–51].

In order to illustrate the dynamic processes in the QDSSCs, the EIS of the TiO_2/CdS/CdSe:Mn^{2+} (or Cu^{2+}) photoanodes are measured. Fig. 4(b) shows the EIS characteristics for the QDSSCs based on the different photoanodes and parameters that are listed in Table 4. R_s is a set of resistance to the charge transfer at Ag/FTO/TiO_2 front contact and Ag/FTO/Cu_2S back contact; R_s values are obtained at about 19.29 Ω for the best photoanodes. The result shows that the applied technique is strongly affected. The R_{CE} is the resistance at the Cu_2S/electrolyte and the FTO/TiO_2 interfaces. The R_{ct} is the resistance against the electron diffusion in TiO_2, the charge recombination resistance at the TiO_2/QDs/electrolyte interface, and against the inside diffusion in the electrolyte (Zw).

Compared with CdSe:Mn^{2+}(Cu^{2+}), a semicircle of a pure CdSe nanoparticle is largely extended, corresponding to the

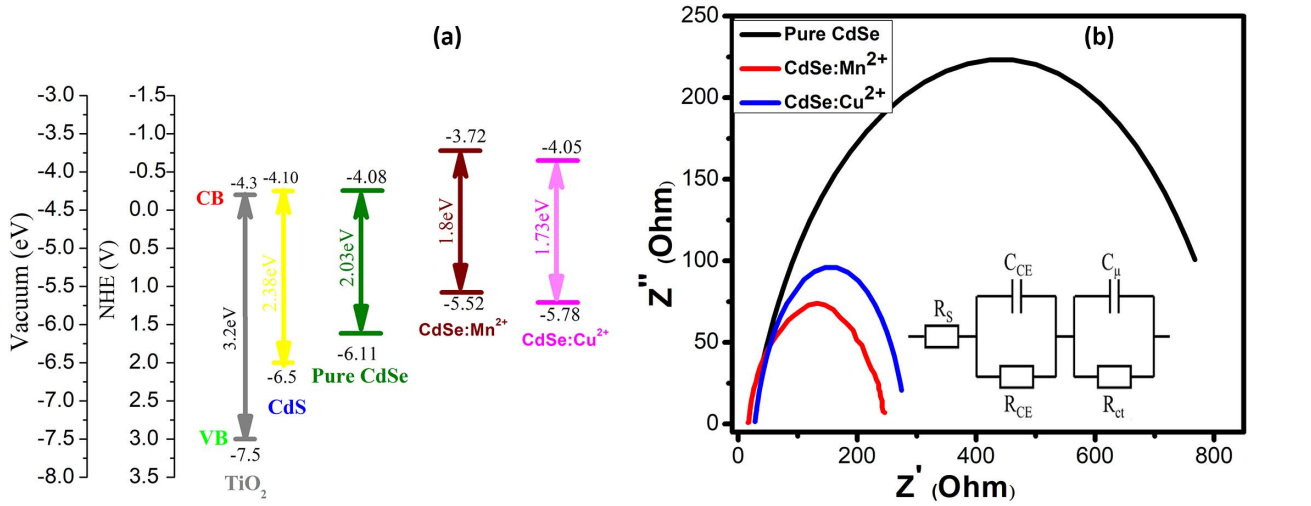

Fig. 4. (a) Schematic diagram for the band alignment in TiO_2/CdS/CdSe:X (Mn^{2+} or Cu^{2+}) QDSSCs and (b) Nyquist curves of pure CdSe and CdSe:X-QDSSCs.

largest R_{ct} (R_{CE}) resistance, which is approximately 194.8 Ω (630.5 Ω), while the C_μ is the smallest (12.25 μF) and the lifetime is the shortest (200 ns). Besides, there was the diminishing of semicircles as X was doped on pure CdSe nanoparticles, and the R_{ct} (R_{CE}) resistances of CdSe:Mn^{2+} and CdSe:Cu^{2+} decreased dramatically from 194.8 to 24.65 and 8.681 Ω (from 630.5 to 204.5 and 254.4 Ω), while there was an upward trend of the C_μ from 12.25 to 120 and 160.5 μF, respectively. It is noticeable that the Mn^{2+}(Cu^{2+}) ions doped on pure CdSe nanoparticles can enhance the light harvesting, generation, collection, and injection of the excited electrons between nanoparticles and TiO_2 film. It is completely suitable with that of the UV-Vis [the CB and VB levels of the CdSe:Mn^{2+} (Cu^{2+}) are estimated and listed in Table 3 with values of −3.74 eV (−4.05 eV), which are higher than both that of pure CdSe (−4.08 eV) and that of CdS (−4.10 eV)].

The CdSe:Mn^{2+} (Cu^{2+}) nanocrystals were synthesized by SILAR. It was found that the CdSe:Mn^{2+} (Cu^{2+}) nanocrystals adopt a blended structure over all of the compositions, and the ternary CdSe:Mn^{2+} (Cu^{2+}) nanocrystals with tunable band gap properties extend the band edge of the optical light absorption from 500 to 610 nm compared to the pure CdSe. The QDSSCs based on the TiO_2/CdS/CdSe:Mn^{2+} (Cu^{2+}) anodes were successfully prepared, which exhibit the high performance: $J_{SC} = 18.99$ mA/cm^2, $V_{OC} = 0.381$ V, FF = 0.52, and $\eta = 3.77\%$ ($J_{SC} = 19.915$ mA/cm^2, $V_{OC} = 0.421$ V, FF = 0.503 and $\eta = 4.22\%$), respectively. This result shows that the Mn^{2+} (Cu^{2+}) ions doped on pure CdSe nanoparticles can increase the light harvesting to produce more excitons, making a fast electron transfer at TiO_2/CdS/CdSe:Mn^{2+} (Cu^{2+})/ZnS/electrolyte interfaces, and the reduced recombination in the QDSSCs as ZnS coating protected nanoparticles. Moreover, the Mn^{2+} (Cu^{2+}) dopant raises the CB levels of CdSe nanoparticles, which are higher than that of CdS nanoparticles, accelerating the exciton injection kinetics in the QDSSCs.

References

1. M. C. Beard, J. Phys. Chem. Lett. **2**, 1282 (2011).
2. P. V. Kamat, J. Phys. Chem. C **112**, 18737 (2008).
3. A. Nozik, J. Phys. E **14**, 115 (2002).
4. S. S. Mali, S. K. Desai, S. S. Kalagi, C. A. Betty, P. N. Bhosale, R. S. Devan, Y.-R. R. Mad, and P. S. Patila, Dalton Trans. **41**, 6130 (2012).
5. J. Jiao, Z.-J. Zhou, W.-H. Zhou, and S.-X. Wu, Mater. Sci. Semicond. Process **16**, 435 (2013).
6. N. P. Benehkohal, V. González-Pedro, P. P. Boix, S. Chavhan, R. Tena-Zaera, G. P. Demopoulos, and I. Mora-Seró, J. Phys. Chem. **1**, 16391 (2012).
7. Q. Zhang, Y. Zhang, S. Huang, X. Huang, Y. Luo, Q. Meng, and D. Li, Electrochem. Commun. **12**, 327 (2010).
8. V. González-Pedro, X. Xu, I. Mora-Seró, and J. Bisquert, ACS Nano **4**, 5783 (2010).
9. Z. Yang and H.-T. Chang, Sol. Energy Mater. Sol. Cells **94**, 2046 (2010).
10. N. Balisa, V. Dracopoulos, K. Bourikas, and P. Lianos, Electrochim. Acta **91**, 246 (2013).
11. D. H. Jara, S. Joon Yoon, K. G. Stamplecoskie, and P. V. Kamat, Chemi. Mater. **26**, 7221 (2014).
12. S. Woo Jung, J.-H. Kim, H. Kim, C.-J. Choi, and K.-S. Ahn, J. Curr. Appl. Phys. **12**, 1459 (2012).
13. T. R. Ravindran, A. K. Arora, B. Balamuruga, and B. R. Mehta, Nanostruct. Mater. **11**, 603 (1999).
14. T. Lopez-Luke, A. Wolcott, L.-P. Xu, S. Chen, Z. Wen, J. Li, E. D. L. Rosa, and J. Z. Zhang, J. Phys. Chem. C **112**, 1282 (2008).
15. I. Mora-Sero, S. Gimenez, T. Moehl, F. Fabregat-Santiago, T. Lana-Villareal, R. Gomez, and J. Bisquert, Nanotechnology **19**, 424007 (2008).
16. Q. Shen, J. Kobayashi, L. J. Diguna, and T. Toyoda, J. Appl. Phys. **103**, 084304 (2008).
17. J.-W. Lee, D.-Y. Son, T. K. Ahn, H.-W. Shin, I. Y. Kim, S.-J. Hwang, M. J. Ko, S. Sul, H. Han, and N.-G. Park, Sci. Rep. **3**, 1050 (2013).
18. P. K. Santra and P. V. Kamat, J. Am. Chem. Soc. **134**, 2508 (2012).
19. L. Zhu, T. X. Pan, and Z. Sun, ACS Appl. Mater. Interfaces **3**, 3146 (2011).
20. Y. H. Lee, S. H. Im, J. A. Chang, J. H. Lee, and S. I. Seok, Org. Electron. **13**, 975 (2012).
21. M. A. Hossain, J. R. Jennings, C. Shen, J. H. Pan, Z. Y. Koh, N. Mathews, and Q. Wang, J. Mater. Chem. **22**, 16235 (2012).

22. Z. Pan, K. Zhao, J. Wang, H. Zhang, Y. Feng, and X. Zhong, ACS Nano **7**, 5215 (2013).
23. J. G. Radich, N. R. Peeples, P. K. Santra, and P. V. Kamat, J. Phys. Chem. C **118**, 16463 (2014).
24. J. Wang, I. Mora-Sero, Z. Pan, K. Zhao, H. Zhang, Y. Feng, G. Yang, X. Zhong, and J. Bisquert, J. Am. Chem. Soc. **135**, 15913 (2013).
25. K. Yan, L. Zhang, J. Qiu, Y. Qiu, Z. Zhu, J. Wang, and S. Yang, J. Am. Chem. Soc. **135**, 9531 (2013).
26. Q. Dai, E. M. Sabio, W. Wang, and J. Tang, Appl. Phys. Lett. **104**, 183901 (2014).
27. T. Debnath, P. Maity, S. Maiti, and H. N. Ghosh, J. Phys. Chem. Lett. **5**, 2836 (2014).
28. Y. L. Le and Y. S. Lo, Adv. Funct. Mater. **19**, 604 (2009).
29. Y. L. Xie, Electrochim. Acta **105**, 137 (2013).
30. C. Xing, Y. Zhang, W. Yan, and L. Guo, Int. J. Hydrogen Energy **31**, 2018 (2006).
31. M. Askari, N. Soltani, E. Saion, W. M. M. Yunus, M. H. Erfani, and M. Dorostkar, Superlattices Microstruct. **81**, 193 (2015).
32. A. S. Hassanien and A. A. Akl, Superlattices Microstruct. **89**, 153–169 (2015).
33. H. T. Tung, N. T. Thao, and L. Q. Vinh, Int. J. Photoenergy **8**, 8545207 (2018).
34. B. S. Bhupendra, S. Jana, and N. Pradhan, J. Am. Chem. Soc. **133**, 1007 (2011).
35. M. P. A. Muthalif, Y. S. Lee, C. D. Sunesh, H. J. Kim, and Y. Choe, Appl. Surf. Sci. **396**, 582 (2016).
36. S. K. Niladri, D. D. Sarma, R. M. Kadam, and N. Pradhan, J. Phys. Chem. Lett. **1**, 2863 (2010).
37. C. Corrado, Y. Jiang, F. Oba, M. Kozina, F. Bridges, and J. Z. Zhang, J. Phys. Chem. A **113**, 3830 (2009).
38. P. Mandal, S. S. Talwar, S. S. Major, and R. S. Srinivasa, J. Chem. Phys. **128**, 114703 (2008).
39. N. Pradhan, D. Goorskey, J. Thessing, and X. Peng, J. Am. Chem. Soc. **127**, 17586 (2005).
40. R. Xie and X. Peng, J. Am. Chem. Soc. **131**, 10645 (2009).
41. R. Beaulac, S. T. Ochsenbein, and D. R. Gamelin, *Nanocrystal Quantum Dots*, 2nd ed. (CRC Press, 2010).
42. A. A. Bol, J. Ferwerda, J. A. Bergwerff, and A. Meijerink, J. Lumin. **99**, 325 (2002).
43. C. Gan, Y. Zhang, D. Battaglia, X. Peng, and M. Xiao, Appl. Phys. Lett. **92**, 241111 (2008).
44. S. Jana, B. B. Srivastava, S. Acharya, P. K. Santra, N. R. Jana, D. D. Sarma, and N. Pradhan, Chem. Commun. **46**, 2853 (2010).
45. B. B. Srivastava, S. Jana, N. S. Karan, S. Paria, N. R. Jana, D. D. Sarma, and N. Pradhan, J. Phys. Chem. Lett. **1**, 1454 (2010).
46. M. P. A. Muthalif, Y. S. Lee, C. D. Sunesh, H. J. Kim, and Y. Choe, Appl. Surf. Sci. **396**, 582 (2016).
47. T. H. Thanh, V. L. Quang, and H. T. Dat, J. Nanomater. 2016, 9806386 (2016).
48. T. T. Ha, C. H. Chi, N. Vy, N. T. Thoa, T. D. Huynh, and Q. V. Lam, Environ. Prog. Sustainable Energy **34**, 1774 (2015).
49. T. H. Thanh, V. L. Quang, and D. H. Thanh, Sol. Energy Mater. Sol. Cells **143**, 269 (2015).
50. T. H. Thanh, L. Q. Vinh, and H. T. Dat, Braz. J. Phys. **44**, 746 (2014).
51. Y. F. Xu, W. Q. Wu, H. S. Rao, H. Y. Chen, D. B. Kuang, and C. Y. Su, Nano Energy **11**, 621 (2014).